Experimental and finite element study on the compression properties of Modified Rectangular Fiber-Reinforced Elastomeric Isolators (MR-FREIs)

Niel C. Van Engelen *, Peyman M. Osgooei, Michael J. Tait, Dimitrios Konstantinidis

Department of Civil Engineering, McMaster University, 1280 Main St. West, Hamilton, Ont. L8S 4L7, Canada

A R T I C L E   I N F O

A B S T R A C T

This study investigates the compressive behavior of Modified Rectangular Fiber-Reinforced Elastomeric Isolators (MR-FREIs). The geometric modifications are introduced to reduce the horizontal stiffness and increase the energy dissipation of the isolation system, allowing long rectangular isolators that provide uniform support along walls to be utilized. It is of critical importance that MR-FREIs maintain adequate vertical stiffness to satisfy the requirements for an isolation system. Experimental data from vertical tests of four rectangular FREIs with and without geometric modifications is used to evaluate a three-dimensional (3D) finite element (FE) model. The 3D FE model is then used to conduct a parametric study on two MR-FREI configurations with varying geometry. The parametric study investigates the effect of the geometric modifications on the vertical stiffness and compression modulus in addition to stress and strain distributions in the elastomer and fiber reinforcement. The study identifies that, similar to annular isolators, introducing a minor geometric modification to the interior of the isolator results in a significant decrease in vertical stiffness and compression modulus. This influence is considerably less for geometric modifications positioned on the exterior of the isolator.

© 2014 Elsevier Ltd. All rights reserved.

1. Introduction

Elastomeric isolators consist of alternating horizontal layers of elastomer and reinforcement. The reinforcement serves primarily to restrain the lateral bulging of the elastomeric layers under vertical compressive stresses. The restraint of the elastomer enhances the vertical stiffness of the isolator due to the near incompressibility of the elastomer, resulting in a vertical stiffness that is significantly greater than the horizontal stiffness. The horizontal stiffness is comparatively uninfluenced by the reinforcement. A high vertical stiffness is necessary for the suppression of a rocking mode which may be introduced by the isolation system. Historically, steel plates in the form of shims have been the reinforcement of choice; however, conventional Steel-Reinforced Elastomeric Isolators (SREIs) are heavy and expensive. The weight is attributed to the steel shims and thick steel end plates used to mechanically fasten the isolator to the supports. The cost is in part due to the highly labor-intensive process required to prepare the steel for bonding to the elastomeric layers [1]. It was proposed by Kelly [2] that the steel reinforcement be replaced with lighter fiber reinforcement of similar mechanical

tensile properties. The concept of Fiber-Reinforced Elastomeric Isolators (FREIs) has been investigated experimentally in numerous studies, including Kelly [2], Moon et al. [3,4], and Toopchi-Nezhad et al. [5,6], and shown to perform well with several distinct advantages, such as superior energy dissipation and, for unbonded FREIs with a sufficiently large width-to-height aspect ratio, a unique stable rollover behavior.

The positioning of FREIs between the upper and lower supports can be in a bonded or unbonded application. In a bonded application, the isolator is bonded to two steel end plates that are mechanically fastened to the supports. In an unbonded application, the thick steel end plates are eliminated, and the isolator is placed between the upper and lower supports with no mechanical restraints. Stable unbonded FREIs exhibit unique stable rollover due to the unbonded application and the lack of flexural rigidity of the fiber reinforcement. In addition to stable rollover, this type of isolator has been shown, through finite element analysis, to have desirable advantages over identical bonded FREIs, such as lower tensile stress demand on the elastomeric layers and on the fiber reinforcement when displaced horizontally [7].

A significant advantage of FREIs is the ability to manufacture large pads and cut individual isolators from the pads to the desired size [2]. Individual FREIs manufactured using this technique have

---

been utilized in numerous experimental studies such as Toopchi-Nezhad et al. [6] and de Raaf et al. [8]. In buildings with structural walls as the lateral-force-resisting system, conventional square or circular isolators are often orientated in a grid pattern and require the use of a structural system to adequately transfer the loads applied to the walls to the isolators. Long rectangular FREIs allow for uniform support to be provided along shear walls [2], which reduces the requirements of a load transfer system. This approach has the potential for significant cost savings in the construction process and is well suited to structures with concrete or masonry shear walls. A comparison of a base-isolated masonry wall using square or circular and rectangular isolators is illustrated in Fig. 1.

The performance of a base isolation system is primarily a function of the horizontal stiffness. The horizontal stiffness should be sufficiently low in order to shift the fundamental period out of the high-energy range of a typical earthquake event and essentially decouple the structure from the ground motion. If long rectangular isolators are used, a relatively high horizontal stiffness is expected due to the large plan area of the isolator, thereby reducing the shift in the fundamental period and, thus, the overall efficiency of the isolation system. In the interest of improving the design of the isolation system, the horizontal stiffness and energy dissipation characteristics can be adjusted through the introduction of geometric modifications to the plan loaded surface. This concept, denoted as Modified Rectangular Fiber-Reinforced Elastomeric Isolators (MR-FREIs), is demonstrated in Fig. 2. Although intended to alter the horizontal performance, the geometric modifications also influence the vertical properties of the isolator relative to an unmodified isolator. It is critical that the rectangular geometry and high vertical stiffness necessary for isolation systems be maintained despite the modifications. Therefore, it is vital to understand how modifications to the plan loaded surface will simultaneously alter both the horizontal and vertical performance of the isolator, including increased stresses and changes in pressure distributions caused by the modifications.

In this paper the effect of modifications to the plan loaded surface on the vertical stiffness and compression modulus of MR-FREIs is investigated. A three-dimensional (3D) Finite Element (FE) model is developed and evaluated using experimental data from four isolators. The model is subsequently used to conduct a parametric study on the influence of the diameter of the circular modifications on the vertical stiffness and compression modulus for two different configurations. Furthermore, the FE model is used to examine the variations in the stress and strain distributions of the elastomeric layers and fiber reinforcement.

2. Background

2.1. MR-FREIs

Selecting an elastomer with a low shear modulus, G_e, alone often permits the targeted horizontal stiffness to be achieved;

however, additional measures may be required for long rectangular isolators. The introduction of modifications will simultaneously decrease the plan loaded area, decrease the shape factor, S, defined as the ratio of the loaded area to the unloaded area of a single layer of elastomer, and modify the pressure distribution. A reduction in plan loaded area directly decreases both the horizontal and vertical stiffness, whereas changes in the shape factor and pressure distribution will also alter the horizontal and vertical behavior of the isolator, as discussed in Van Engelen et al. [9].

It is common for shape factors greater than approximately 5 to assume that the stress within the elastomeric layers is dominated by the internal pressure, known as the pressure solution [10]. This assumption is often made in analytical solutions for rectangular and circular elastomeric isolators [2,10-17], although analytical solutions exist that relax this assumption, such as Pinarbasi and Mengi [18] and Tsai [19,20]. Modifications can significantly alter the pressure distribution depending on the orientation, resulting in areas of higher stress concentrations. Therefore, changes in the pressure distribution as a result of the modifications are also expected to influence the horizontal and vertical properties.

Modifications will decrease the shape factor since the unloaded area increases and the plan loaded area decreases simultaneously, which both act to reduce the shape factor. It has been shown through analytical solutions that the vertical stiffness of rectangular FREIs [16] and horizontal stiffness of infinite strip FREIs [21,22] are influenced by the shape factor. In a FE study, the compression modulus for unmodified unbonded FREIs was shown to have a greater rate of increase than the rate of increase of the shape factor, rendering the shape factor an important design parameter [23].

A preliminary study on the vertical stiffness and compression modulus of MR-FREIs was conducted by Van Engelen et al. [24]. The purely experimental study considered six specimens with three modification configurations and two modification diameters. The test results showed that a substantial drop in vertical stiffness occurred with minor modification, but that the decrease was dependent on the configuration of the modification. Similar trends observed with the vertical stiffness were noted with the compression modulus, but to a lesser degree, suggesting that the shape factor and pressure distribution are important considerations.

The effective horizontal stiffness and energy dissipation characteristics of four isolators presented in Van Engelen et al. [24] were experimentally examined in Van Engelen et al. [9] over a displacement range of 0.25 t_r to 2.50 t_r, where t_r is the total thickness of the elastomeric layers. The study, which only considered isolators with holes placed in the interior of the plan area, indicated that the effective horizontal stiffness and equivalent viscous damping, in comparison to the control specimen, were dependent on the horizontal displacement. With the exception of large displacements, i.e., 2.00 t_r to 2.50 t_r, the decrease in effective horizontal stiffness was larger than the decrease in the plan loaded area of the specimen. The equivalent viscous damping was found to increase at all displacement amplitudes considered in comparison to the control specimen. The increase in damping was attributed to the
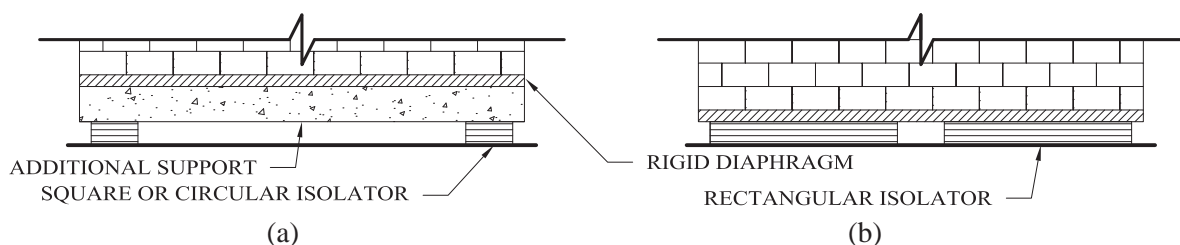

Fig. 1. Isolation system supporting a masonry wall with (a) localized square or circular isolators and (b) large rectangular isolators that provide uniform support.
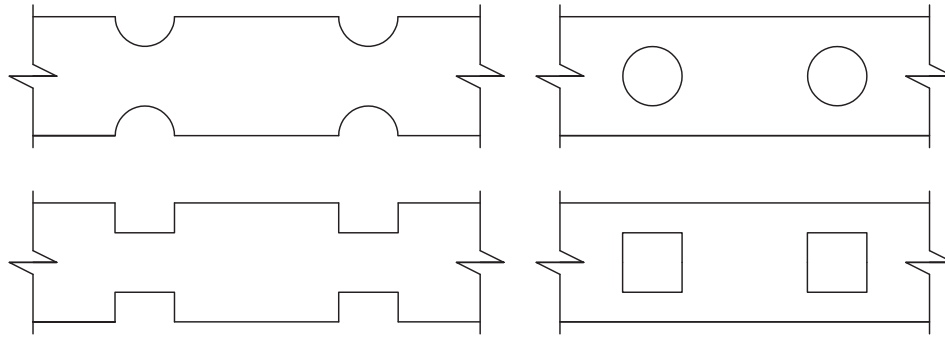
Fig. 2. Plan view of potential MR-FREI designs.

decrease in effective horizontal stiffness and a decrease in the length of the fiber reinforcement. It was postulated in the study that the modifications allowed for an increase in inter-fiber movement causing an increase in the energy dissipation characteristics of the isolator.

In a FE study conducted by Dezfuli and Alam [25], it was shown that the vertical stiffness of FREIs reinforced with carbon fiber was more sensitive to changes in the shear modulus, thickness of the fiber reinforcement and number of elastomeric layers than the effective horizontal stiffness or equivalent viscous damping. In that study, the total height was held constant, thus the number of elastomeric layers is also representative of the shape factor since an increase in the number of layers requires a decrease in the layer thickness resulting in a larger shape factor. Utilizing FE analysis, Toopchi-Nezhad et al. [23] identified that the compression modulus was highly sensitive to changes in the shape factor, while the horizontal stiffness was not. The preliminary findings in Van Engelen et al. [9,24] suggest that the decrease in the vertical properties due to the modifications can be significant. Therefore, assessing the effect of various design parameters is critical to accurately characterizing the vertical behavior of MR-FREIs.

2.2. Annular isolators

Modifications have been investigated analytically for circular SREIs and FREIs in the form of annular isolators. Constantinou et al. [11] developed a factor to take into consideration the addition of a circular hole at the center of a circular SREI forming an annular isolator. Fig. 3 shows the profile view of a section of a circular and annular isolator with an outer radius, R_1, and inner radius, R_2. The introduction of the modification creates an additional free surface where lateral bulging occurs. As the ratio of R_2/R_1 for an annular isolator with an incompressible elastomer approaches unity, the compression modulus, E_c, initially that of a circular isolator, $E_c = 6GS^2$, converges to the solution of an infinite strip isolator, $E_c = 4GS^2$. The compression modulus drops abruptly at small values of R_2/R_1 and quickly converges to the solution of an infinite strip isolator.
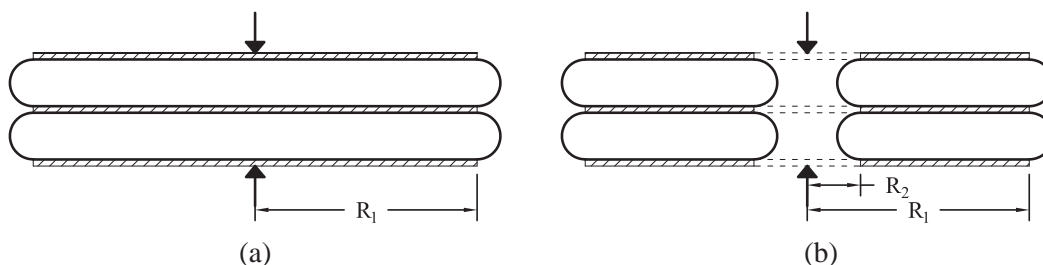
Due to this rapid convergence, it has been indicated that regardless of the size of the central hole, the compression modulus for annular isolators should conservatively be taken as the solution for an infinite strip isolator, $E_c = 4GS^2$ [14].

An analytical study conducted by Pinarbasi and Okay [17] investigated the performance of annular FREIs focusing on four key parameters: the reinforcement extensibility, modification diameter, shape factor and elastomer compressibility. The deformed shape was defined according to the assumptions of the pressure solution. An additional displacement term was included to capture the extensibility of the fiber reinforcement and the compressibility of the elastomer was also considered. The study concluded that E_c drops abruptly with the introduction of a minor modification for incompressible elastomers, similar to the analytical solution obtained for SREIs. The magnitude of the drop decreases with compressibility, especially for isolators with a high shape factor where the restraint effect is reduced due to the compressibility.

3. Experimental testing

3.1. Isolator design

The isolators considered in this study are of the same geometry and layer design as four of the isolators used in Van Engelen et al. [9,24]. The isolators were manufactured in large pads and subsequently cut to the desired plan dimensions with a width, $(2a)$, of 76 mm and length, $(2b)$, of 52 mm, as illustrated in the plan and profile view in Fig. 4. The quarter scale layer design is identical to the design described in Foster [26]. The isolators contained seven layers of Neoprene; the five interior layers of elastomer had a thickness of 3.18 mm, and the two exterior layers of elastomer had a thickness of 1.59 mm. Bidirectional plain weave carbon fiber reinforcement with a 0.25 mm thickness was bonded to the elastomer. After bonding, the reinforcement layer thickness was approximately 0.55 mm for a total thickness of elastomeric layers of 19.05 mm, and a total height, h, of 22.35 mm.
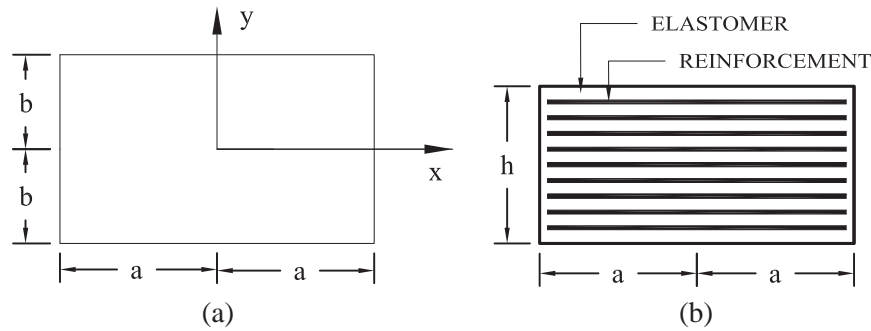

Fig. 3. Profile view of the lateral bulging of (a) a circular isolator and (b) an annular isolator.

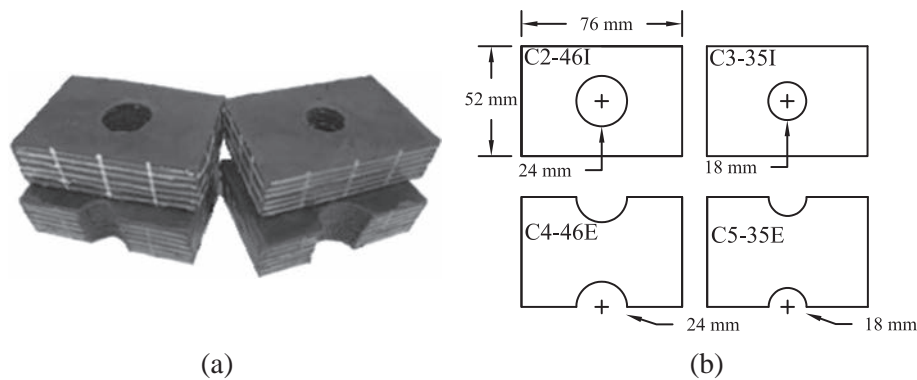**Fig. 4.** (a) Plan and (b) profile view of a FREI.

Fig. 5. (a) Photograph and (b) plan view of the specimens.

A plan view of the four specimens considered and the test spec-imens are shown in Fig. 5. Two modification configurations and two diameters were considered. The geometric characteristics of the specimens considered are summarized in Table 1. The modifi-cations were circular with a diameter, d, of 18 mm and 24 mm, or normalized by the length, $d/2b = 0.35$ and 0.46, respectively. The specimens are numbered C2 through to C4. If the specimen has been modified, a designation is included after the specimen num-ber. The designation represents the normalized diameter of the modification, $d/2b$, expressed as a percent and placement of the modification as interior, I, or exterior, E. For example, C2-46I refers to specimen C2 with an interior modification of $d/2b = 0.46$. As shown in Fig. 5b, Specimen C2-46I and C3-35I each had a single cir-cular modification placed at the geometric center of the isolator, referred to as an interior modification. Specimen C4-46E and C5-35E had a half-circle modification removed from each side of the isolator at the center of the 76 mm width, referred to as an exterior modification. By placing modifications on the interior and exterior, isolators of identical loaded area but different shape factors can be analyzed. The modifications reduced the loaded area of the specimens by 6.4% and 11.4% for the $d/2b = 0.35$ and 0.46 modifications, respectively.

Table 1
Specimen geometric characteristics.

Specimen	Area (mm²)	S		$d/2b$	Area removed (%)
		Interior	Exterior		
Unmodified	3952	4.9	9.7	–	–
C2-46I	3500	3.3	6.7	0.46	11.4
C3-35I	3698	3.7	7.5	0.35	6.4
C4-46E	3500	3.9	7.8	0.46	11.4
C5-35E	3698	4.2	8.4	0.35	6.4

3.2. Experimental setup and vertical test procedure

A photograph and schematic of the experimental test apparatus emphasising the components for vertical tests are shown in Fig. 6. The setup was configured to conduct horizontal displacement con-trolled and vertical load-controlled tests. The vertical load was applied to a steel plate and distributed to three identical load cells. The specimen was situated between two steel plates, and the ver-tical displacement was measured at four locations between the upper and lower platen with laser displacement transducers. The lower platen was on linear bearings and connected to a horizontal actuator, a brace on the upper platen provided the reaction force to the horizontal actuator during horizontal tests. Each isolator was placed unbonded into the setup between two level steel plates.

The compressive force was selected assuming application of the isolators on a structure similar to those considered in experimental tests conducted by Foster [26] and Toopchi-Nezhad et al. [27]. In the test program, the load was held constant for all specimens to simulate the application of the isolators on an identical structure. The loading was conducted according to procedures outlined in ISO-22762 [28]. Each specimen was monotonically loaded to a compressive force of 7.9 kN at zero horizontal displacement, which corresponds to an average vertical compressive stress of $\bar{p} = 2.0$ MPa for the unmodified specimen plan area. Once the com-pressive load was achieved, it was fluctuated ±20% over three sinu-soidal cycles at a frequency of 0.2 Hz and then monotonically unloaded, as shown in Fig. 7 for an unmodified isolator. Each spec-imen was initially tested unmodified and visually inspected for damage. The modifications were then introduced, and the speci-mens were re-tested following the same procedure at an average vertical stress of 1.0 MPa and 2.0 MPa according to the unmodified area and visually inspected for damage after each experiment.
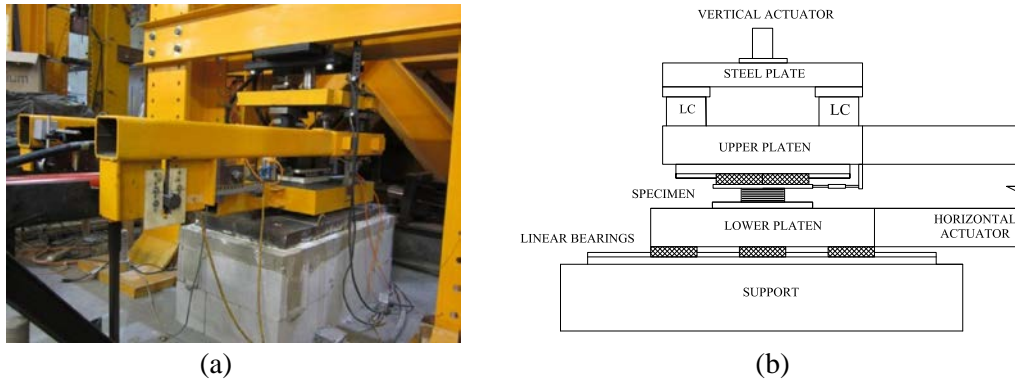
(a)　　　　　　　　　　　　　(b)

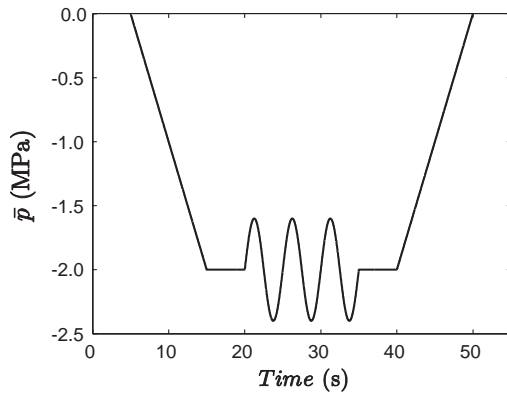**Fig. 6.** (a) Photograph and (b) schematic of the test apparatus.

Fig. 7. Compression test time history for an unmodified isolator.

Fig. 8. Unmodified specimen C2 experimental results showing the compression modulus determined from the third cycle.

The vertical tests in this study were all conducted at zero horizontal displacement, and the properties with horizontal deformation were not considered. The influence of horizontal displacement on low-damping rubber and lead-rubber bearings was experimentally investigated in Warn et al. [29]. The study concluded that the vertical stiffness of the bearings considered decreased with increasing horizontal displacement. A similar decrease in vertical stiffness is expected in MR-FREIs with increasing horizontal displacement.

3.3. Experimental results

The vertical stiffness was determined by using the third cycle maximum and minimum force, P, and maximum and minimum displacement, δ_v, observed over the cycle [28]. The vertical stiffness, k_v, is:

$$k_v = \frac{P_{max} - P_{min}}{\delta_{v,max} - \delta_{v,min}} \tag{1}$$

The compression modulus is determined by:

$$E_c = \frac{k_v t_r}{A} \tag{2}$$

where A is the plan loaded area.

Fig. 8 presents the average vertical stress as a function of the vertical compressive strain for the unmodified isolator C2. The slope of the dashed line is representative of the compression modulus of 108 MPa obtained for the third cycle using Eqs. (1) and (2). All isolators considered displayed some degree of run-in prior to developing the vertical stiffness. The level of run-in is a function of the development of stresses within the fiber reinforcement
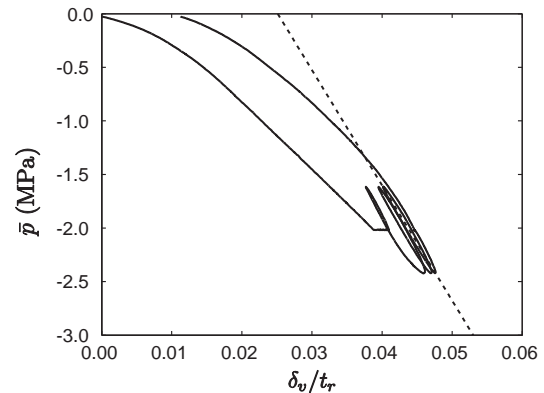
which may not be initially taut [6,12] and potential strain sensitivity of the elastomer. Table 2 shows the vertical stiffness and compression modulus values, where E is the elastic modulus of the elastomer, for the unmodified and modified specimens. The unmodified isolator performance was consistent for the four isolators considered and overall good agreement was obtained with a mean, μ, of 101 MPa, standard deviation, σ, of 5 MPa, and coefficient of variation, c_v, of 0.05.

4. Finite element modeling

4.1. Model development

The 3D FE analysis was conducted using MSC Marc [30], a general purpose commercially available FE software. Both the elastomeric and fiber reinforcement layers were modeled using eight-node linear full integration isoparametric hexahedron elements. The compressible *Neo-Hookean* constitutive model was used to describe the elastomer. This material model is characterized by the shear and bulk moduli of the elastomer. The fiber reinforcement materials were modeled using a linear-elastic isotropic material model.

Table 2
Experimental results.

Property		C2	C3	C4	C5	μ	σ	c_v
$(k_v t_r)/(4Eab)$	Unmodified	67	58	61	61	62	4	0.06
	Modified	37	39	51	52		–	
E_c (MPa)	Unmodified	108	98	97	102	101	5	0.05
	Modified	67	69	91	93		–	

Table 3
Material properties.

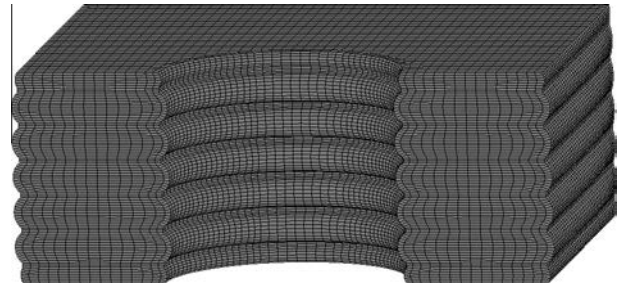| Elastomer	Reinforcement
G_e = 0.6 MPa	E_f = 23 GPa
K_e = 2000 MPa	v_f = 0.2

Table 3 gives the material properties used in the FE analysis where K_e is the bulk modulus of the elastomer and E_f and v_f are the elastic modulus and Poisson's ratio of the fiber reinforcement. A bulk modulus of K_e = 2000 MPa was selected for the Neoprene elastomer. The shear modulus of the Neoprene used in the FE analysis was based on the experimental test results of the unmodified isolators.

The top and bottom supports were modeled using rigid surface elements. A *glue* contact was defined between the rigid surfaces and the top and bottom elastomer layers to prevent any slip along the interface. The hexahedron elements used to model elastomeric layers use a mixed formulation to overcome the numerical difficulties associated with the near incompressibility of the elastomeric material [30]. Fig. 9 shows the FE model of C4-46E highlighting the element size.

4.2. Model evaluation

Fig. 10 shows a cross section of the deformed shape of C2-35I obtained from FE analysis. Similar to the experimental program, the FE analysis was conducted using a constant load determined from $\bar{p}$ based on the unmodified plan area and the vertical stiffness was calculated using Eq. (1). Table 4 compares the experimental and FE analysis ratios of the modified-to-unmodified vertical stiffness. The Neoprene used in these isolators was found to be nonlinear, with a stiffening behavior observed under larger vertical compressive stresses that occur due to the reduced plan area. The 8.6% average error between the FE predictions and test results can partially be attributed to this nonlinear behavior. A more sophisticated constitutive model than the compressible Neo-Hookean model used in this study is required for the elastomeric material in order to capture this stiffening behavior in the FE analysis. However, the 13.3% maximum error between the FE analysis and experimental results was deemed acceptable given the limitations of the material model.

The average compression modulus of the unmodified isolators from the experimental tests was E_c = 101 MPa. The closed form solution derived by Tsai and Kelly [16] was used to estimate the compression modulus of the unmodified isolator. From Tsai and Kelly [16], with the material properties given in Table 3, the compression modulus of the elastomer pads with thicknesses of 3.18 mm and 1.59 mm were calculated as E_c = 90 MPa and E_c = 347 MPa, respectively. The closed form solution derives the compression modulus using a single elastomeric layer that is assumed to be perfectly bonded to flexible reinforcement. In reality, the isolator is composed of a finite number of elastomeric

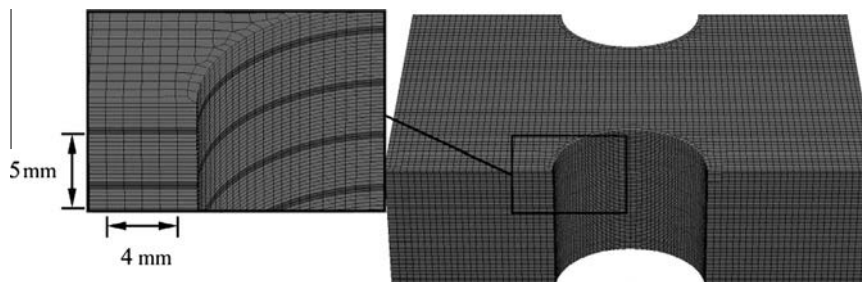**Fig. 10.** Deformed shape cross section of C2-35C at the design load.

Table 4
Comparison of the experimental and FE analysis ratios of modified to unmodified vertical stiffness.

Specimen	Experimental	FE	Error (%)
C2-46I	0.55	0.50	9.1
C3-35I	0.66	0.59	10.6
C4-46E	0.83	0.72	13.3
C5-35E	0.85	0.86	1.2

layers and the contact of the elastomer and the end supports, which are usually assumed to be rigid in comparison to the flexible reinforcement, will affect the vertical response of the isolator. Neglecting the effects of the rigid end boundary condition of the supports on the vertical response of the isolator, the total compression modulus of the isolator can be calculated by treating the elastomeric layers as springs in series. Using this approach, it was calculated that E_c = 103 MPa, which is 2.0% higher than the FE analysis result. It should be noted that considering the bulk compressibility of the elastomer would reduce the predicted value of vertical stiffness. Also, considering the rigid end condition would increase the predicted vertical stiffness value. Osgooei et al. [31] showed that neglecting the rigid end condition in a circular isolator with S = 5 can reduce the vertical stiffness value by 8.5%. Therefore, the results obtained from FE are considered to be in good agreement with the experimental results and analytical solution, and the FE model was deemed appropriate for proceeding with the parametric study.

5. Parametric study

A parametric study was conducted to determine the influence of modifications on the vertical stiffness, compression modulus, and stress and strain distributions. The study considered isolators with interior and exterior circular modifications with diameters ranging between $d/2b$ = 0 and $d/2b$ = 0.58.
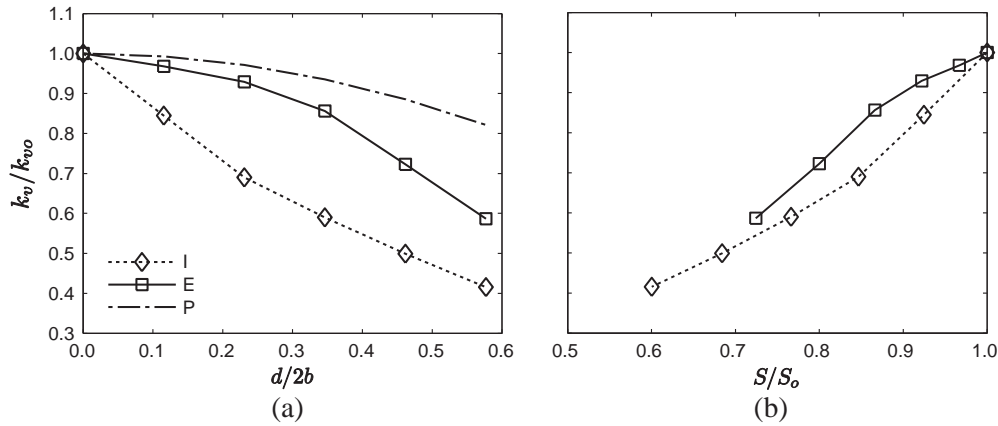

Fig. 9. FE model of C4-46E.

Fig. 11. Normalized vertical stiffness as a function of (a) normalized diameter and (b) normalized shape factor.

5.1. Vertical stiffness

Fig. 11 shows the vertical stiffness of the modified isolators normalized by the unmodified isolator vertical stiffness, k_{vo}, as a function of $d/2b$ and S/S_o, where S_o is the unmodified shape factor. Fig. 11a includes the vertical stiffness of an isolator that is directly proportional to the area removed (P). It can be seen that both interior (I) and exterior (E) modifications result in a larger decrease in normalized stiffness than can be attributed to the reduction in area alone. The interior modification results in a significant decrease even at low values of $d/2b$. For example, at $d/2b = 0.12$ an interior modification has $k_v/k_{vo} = 0.84$, in comparison to the exterior modification for which $k_v/k_{vo} = 0.97$. The exterior modification normalized stiffness is comparable to the proportional area normalized stiffness of $k_v/k_{vo} = 0.99$. The interior modification trend is concave upwards while the exterior modification trend is concave downwards. The contrasting behavior results in a maximum difference in normalized stiffness of 0.27 at $d/2b = 0.35$ and reduces to 0.17 at the maximum considered normalized diameter of $d/2b = 0.58$. The minimum normalized stiffness was 0.42, 0.59 and 0.82 over the range considered for the interior, exterior and proportional representations, respectively. Fig. 11b shows k_v/k_{vo} as a function of S/S_o. The change in S for interior modifications is larger than that of exterior modification with the same diameter. Consequently, the difference between interior and exterior modifications is reduced and begins to converge as S/S_o decreases.

5.2. Compression modulus

Similar to the vertical stiffness, the introduction of an interior modification results in an abrupt decrease in normalized compression modulus, E_c/E_{co}, as shown in Fig. 12, where E_{co} is the unmodified isolator compression modulus. The magnitude E_c/E_{co} is larger than the respective normalized stiffness values with equal diameters, indicating that the compression modulus is less sensitive to the modifications. The minimum relative compression modulus was 0.51 and 0.71 for interior and exterior modifications, respectively. It is interesting to note that the relative compression modulus of 0.85 for an interior diameter of $d/2b = 0.12$ is not surpassed until a diameter of $d/2b = 0.46$ for an exterior modification. This demonstrates that the diameter of the exterior modification can be several times larger than an interior modification and still achieve a comparable compression modulus. Similar to the vertical stiffness, the compression modulus of the interior and exterior modifications begins to converge as the diameter is increased. In the limit, as $d/2b$ approaches unity, the isolator approaches two individual isolators and the influence of the modification configuration diminishes.

The shape factor initially decreases at a larger rate for interior modifications than exterior modifications, as illustrated in Fig. 13. The shape factor for interior modifications is nearly inversely proportional to the diameter. Initially, exterior modifications result in a small change in the shape factor. An exterior modification
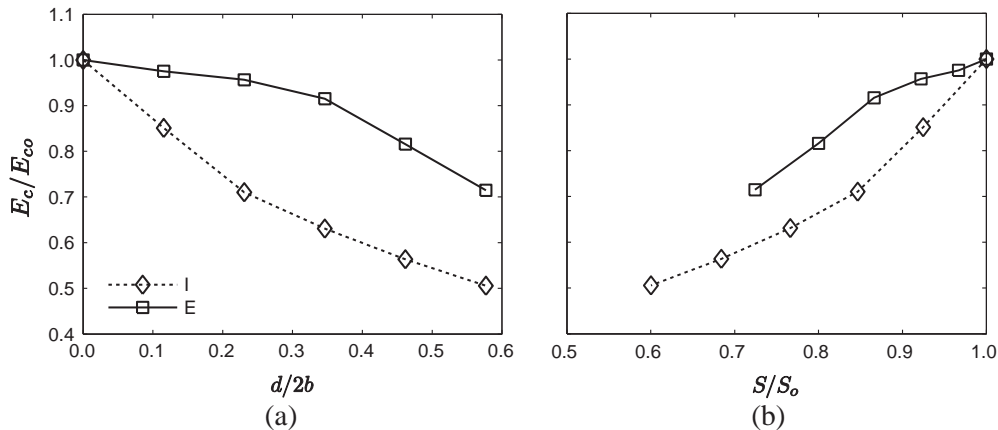

Fig. 12. Normalized compression modulus as a function of (a) normalized diameter and (b) normalized shape factor.
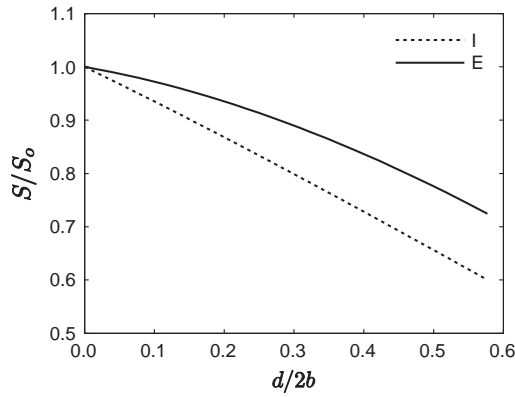
Fig. 13. Normalized shape factor as a function of normalized diameter.

removes a portion of the unloaded area equal to $2dt$, where t is the thickness of the elastomeric layer, but increases the unloaded area by πdt for a total increase of $dt(\pi - 2)$. In comparison, an interior modification adds an unloaded area of πdt without removing any of the existing unloaded area. Therefore, with equal diameters, the change in the interior modification shape factor is more aggressive due to the larger unloaded area. The lower shape factor is representative of a reduction in the restraint of the elastomer by the fiber reinforcement and is believed to be in part responsible for the larger sensitivity of the interior modifications.

5.3. Vertical strain

Fig. 14a and b plot FE results of the vertical strain, ε_{zz}, at the center of the mid-height elastomer layer with interior modifications

where 0 represents the center of the isolator and 1 the respective edge. It can be seen that for the unmodified isolator, with the exception of the edges where lateral bulging occurs, the vertical strain is nearly constant across segments AA and BB. This is in conformance with the assumption in the pressure solution that horizontal planes remain horizontal. Furthermore, the strain in the modified specimens also remains nearly constant. The interior modification caused an increase in the normalized vertical strain in the elastomeric layer. As the diameter increases, the rate of increase in the vertical strain also increases, which is primarily attributed to the increasing rate of area removed.

Fig. 14c and d compare ε_{zz} in the mid-height elastomer layer for exterior modifications. Similar to interior modifications, as the diameter increases, the rate of increase in ε_{zz} increases. The magnitude of the strain for exterior modifications is significantly less than interior modifications. Introducing a $d/2b = 0.12$ exterior modification results in a 4% increase in the average ε_{zz}, which is notably lower than the 36% increase in ε_{zz} observed in the isolator with an equal diameter interior modification. Fig. 15 shows the average ε_{zz}, ignoring the lateral bulging at the edges, as a function of the percent of area removed. It can be seen that the average ε_{zz} is nearly a linear function of the area removed, with the exception of interior modifications, where an abrupt increase in strain magnitude occurs with a minor amount of area removed.

5.4. Vertical stress

Fig. 16a and b compare the normalized vertical stress distribution, $S_{zz}/\overline{p}$, where S_{zz} is the vertical stress at the center of the mid-height elastomer layer, for isolators with interior modifications. Introducing the interior modification alters the vertical stress distribution significantly along both segments. An overall decrease in the magnitude of $S_{zz}/\overline{p}$ was observed along both segments at a
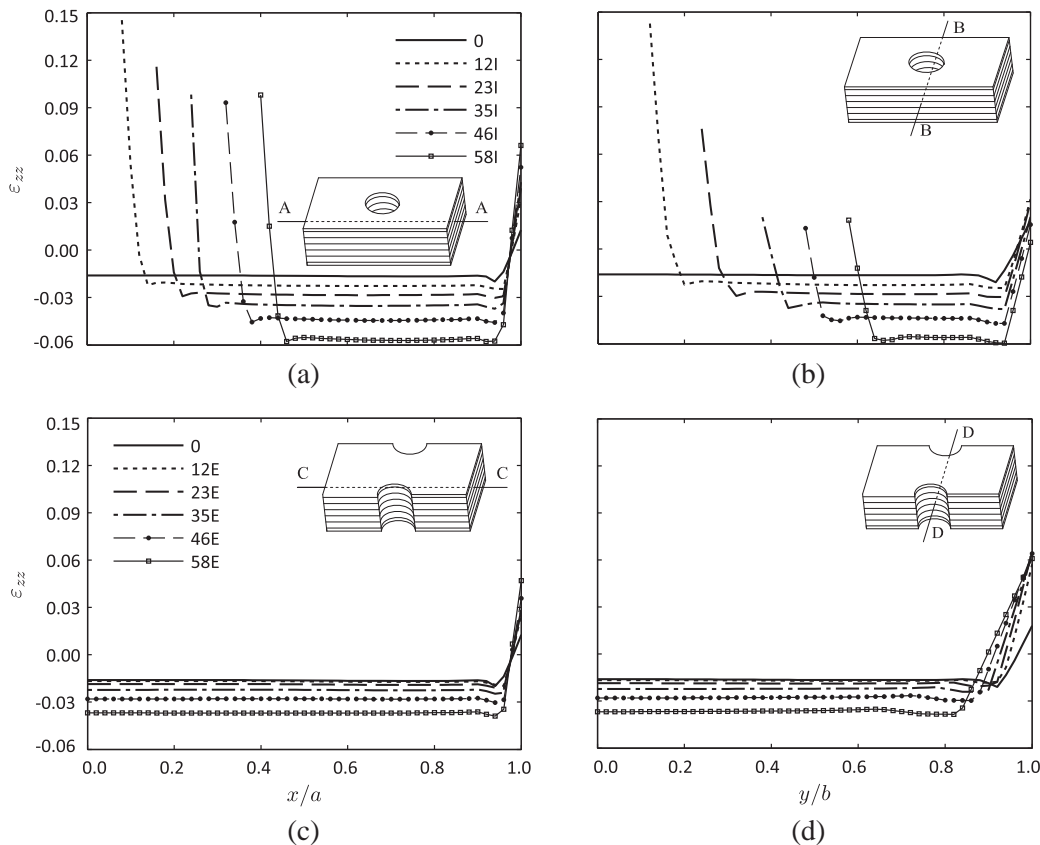

Fig. 14. Vertical strain distribution along the respective segments at the center of the mid-height elastomer layer.
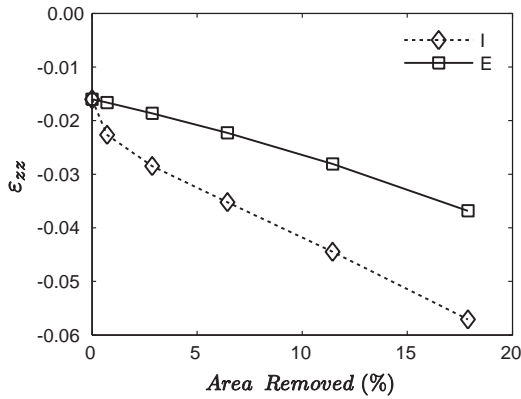
Fig. 15. Average vertical strain as a function of area removed.

diameter of $d/2b = 0.12$. As the diameter increases, $S_{zz}/\bar{p}$ along segment AA increases, exceeding the peak $S_{zz}/\bar{p}$ of the unmodified isolator at a diameter of $d/2b = 0.46$. Along segment BB, however, the magnitude of the peak $S_{zz}/\bar{p}$ continues to decrease with increasing diameter. As the diameter increases, the width of the two portions of the isolator that segment BB crosses become small. As a consequence, the distance to a free edge is reduced, reducing the restraint effect of the reinforcement. Due to the loss of restraint in these regions the primary vertical load resistance is supplied by the ends of the isolator on either side of segment BB.

Fig. 16c and d show the $S_{zz}/\bar{p}$ distribution at the center of the mid-height elastomer layers for isolators with exterior modifications. Initially, the introduction of exterior modifications has little influence over the vertical stress distribution with only a modest increase in peak $S_{zz}/\bar{p}$ along both segments up to a diameter of $d/2b = 0.35$. At a diameter of $d/2b = 0.46$, two peaks of equal

magnitude occur along segment CC. The emergence of these two peaks is representative of the response of the isolator approaching two individual isolators. Along segment DD, it can be seen that the small diameter modifications cause a slight increase in the peak $S_{zz}/\bar{p}$, but a minor decrease along the majority of the segment. As the diameter increases, a substantial drop in vertical stress is observed along the entire segment, indicative of reduced restraint in the center of the isolator and the response approaching two individual isolators.

5.5. Shear stress

Figs. 17 and 18 show the S_{xz} shear stress contours normalized by $\bar{p}$ at the interface of the center elastomer layer and fiber reinforcement for isolators with interior and exterior modifications, respectively. A peak $S_{xz}/\bar{p}$ value of 0.17 was observed in the unmodified isolator. As described earlier, the modifications create an additional free surface that allows additional lateral bulging and increased shear stresses to develop in the vicinity of the modification. For interior modifications, the peak $S_{xz}/\bar{p}$ value occurs near the edge of the modification, whereas for exterior modifications the peak $S_{xz}/\bar{p}$ value occurs at either end of the isolator, similar to an unmodified isolator. Large $S_{xz}/\bar{p}$ values are also observed near the edges of the modifications. With a modification diameter of $d/2b = 0.23$, the peak $S_{xz}/\bar{p}$ value increased by 92.6% for interior modifications (Fig. 17) in comparison to a 13.2% increase for exterior modifications (Fig. 18). At the maximum considered modification diameter of $d/2b = 0.58$, the peak $S_{xz}/\bar{p}$ value increased by 149.8% and 76.6% for interior and exterior modifications, respectively. A peak $S_{xz}/\bar{p}$ value of 0.42 was observed for the interior modification $d/2b = 0.58$.

The normalized S_{yz} shear stress contours are shown in Figs. 19 and 20 for interior and exterior modifications, respectively. Similar to the $S_{xz}/\bar{p}$ contours, significant shear stresses develop in the
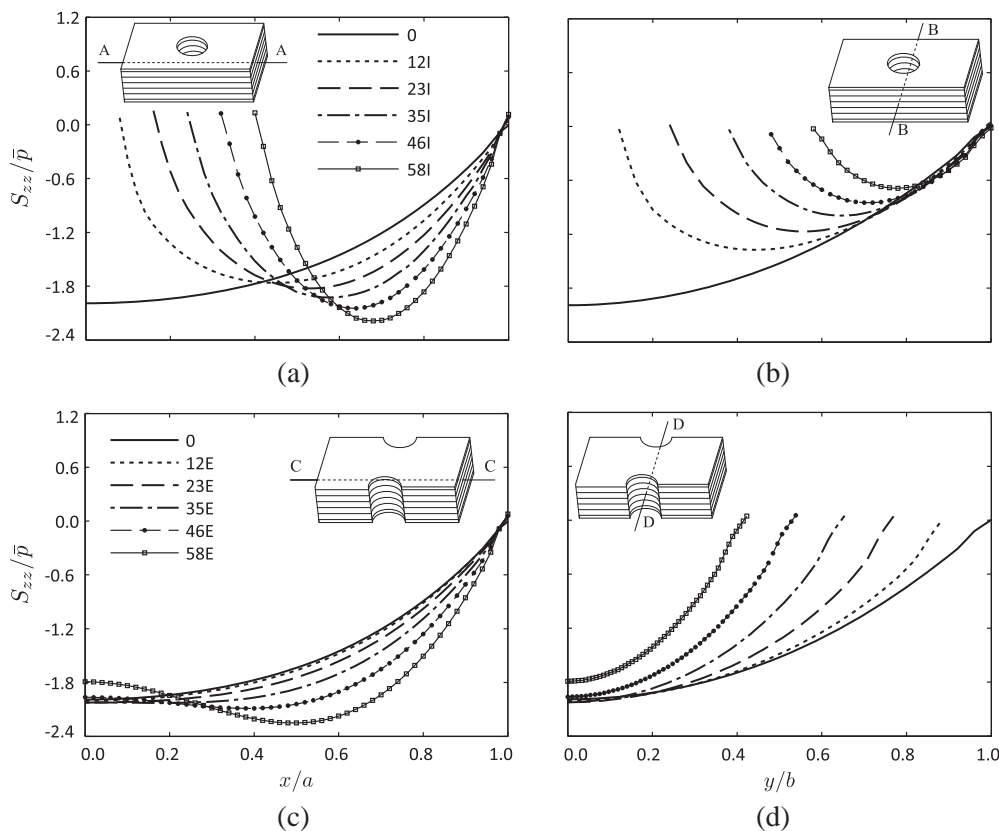

Fig. 16. Normalized vertical stress distribution along the respective segments at the center of the mid-height elastomer layer.

vicinity of the modifications. A peak $S_{yz}/\overline{p}$ value of 0.19 was observed in the unmodified isolator. The peak $S_{yz}/\overline{p}$ value occurs near the edge of the modification for $d/2b$ = 0.23 and 0.35, and near the outer edge of the isolator for the largest considered interior modification, $d/2b$ = 0.58. For the exterior modification, the peak $S_{yz}/\overline{p}$ value occurs near the modification. A modification diameter

of $d/2b$ = 0.23 resulted in a similar increase in peak $S_{yz}/\overline{p}$ value of 40.2% and 41.1% for interior and exterior modifications, respectively. A maximum increase of 64.4% and 78.8% was observed for interior and exterior modifications, respectively. A peak $S_{yz}/\overline{p}$ value of 0.34 was observed for the exterior modification at $d/2b$ = 0.58.
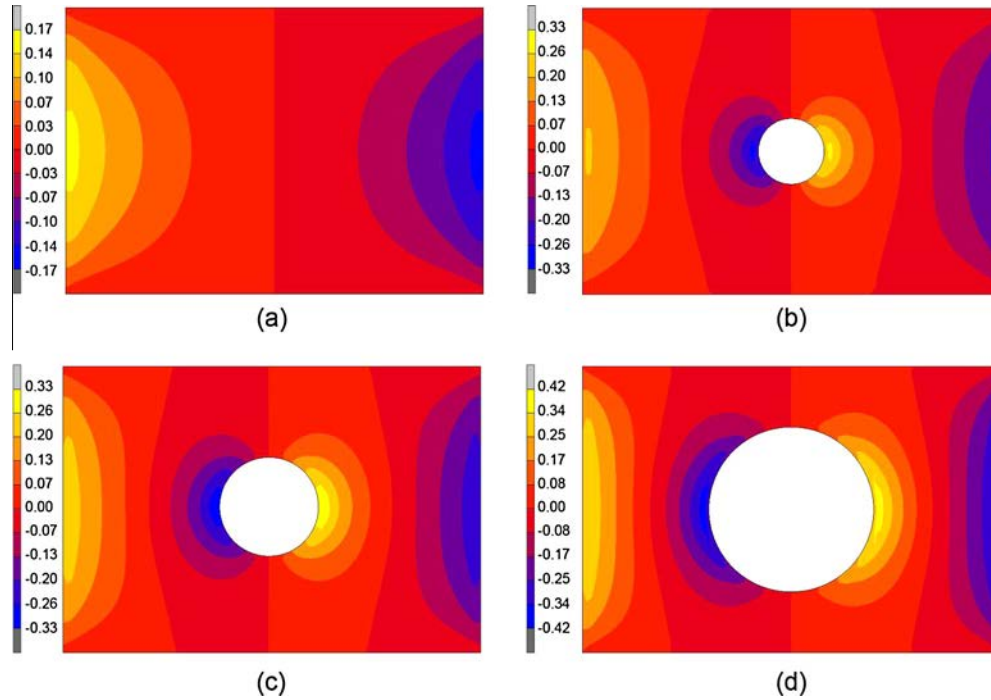

Fig. 17. Normalized S_{xz} shear stress contours at the interface of the center elastomeric layer and fiber reinforcement for isolators with interior modification diameter $d/2b$ = (a) 0, (b) 0.23, (c) 0.35 and (d) 0.58.
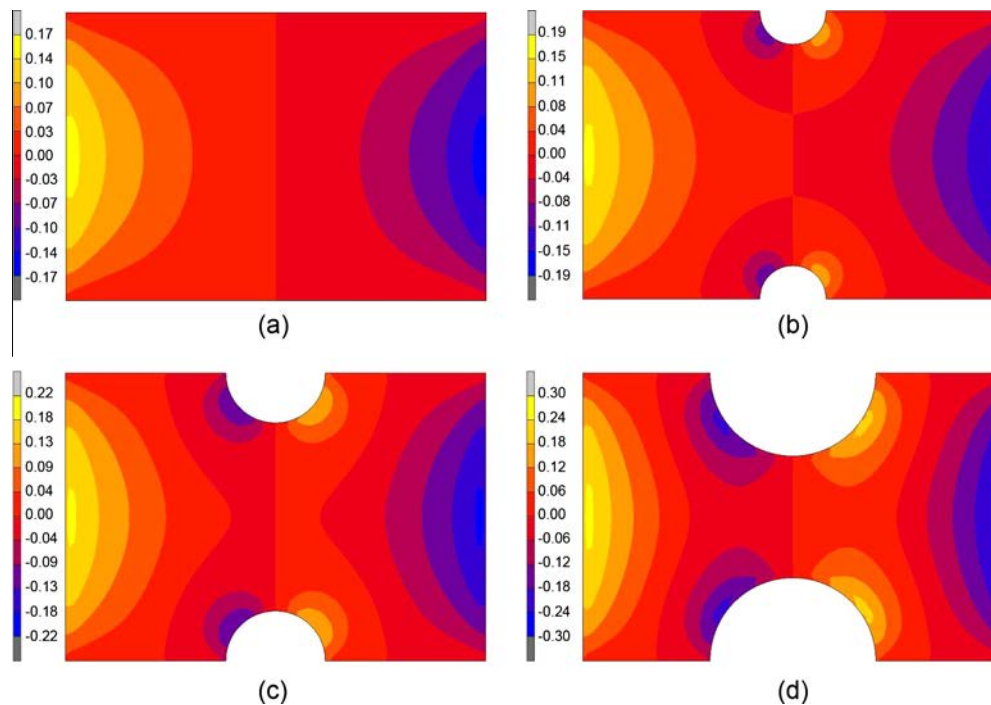

Fig. 18. Normalized S_{xz} shear stress contours at the interface of the center elastomeric layer and fiber reinforcement for isolators with exterior modification diameter $d/2b$ = (a) 0, (b) 0.23, (c) 0.35 and (d) 0.58.

In all modification diameters considered, the overall peak shear stress was observed in S_{xz} for interior modifications and in S_{yz} for exterior modifications. The peak shear stress was larger for all diameters considered for the interior modification in S_{xz} and the exterior modification in S_{yz}. The magnitude of the peak stress in both directions, S_{xz} and S_{yz}, was larger for interior modifications at all diameters considered. Therefore, the shear stresses in the isolators considered in this study with interior modification are more sensitive to the modifications, although significant increases occurred in both geometries.
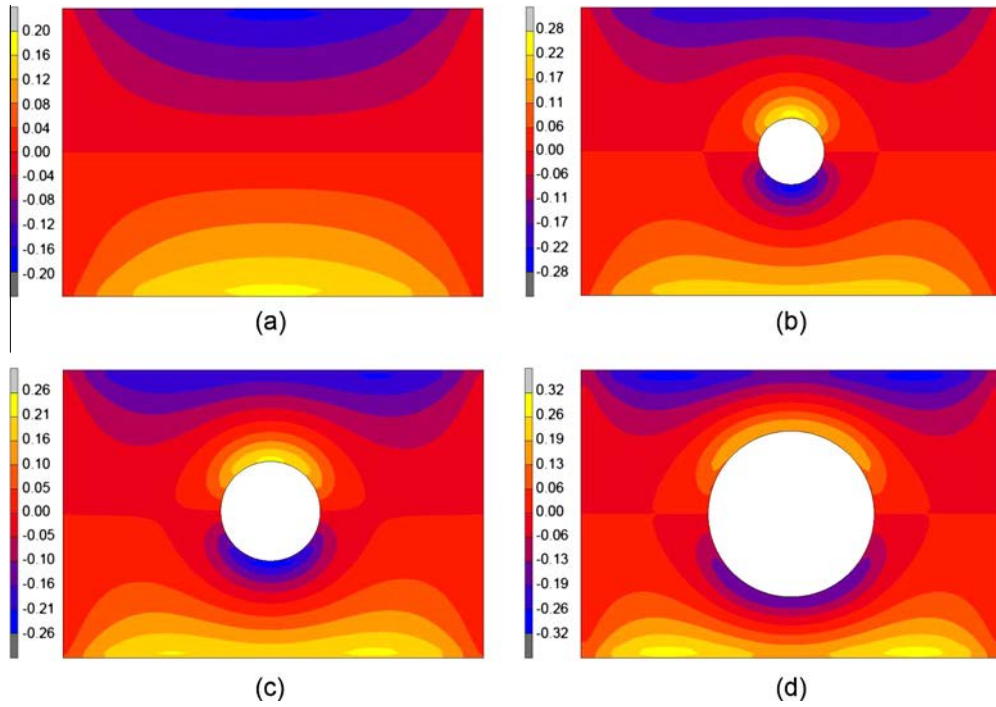

Fig. 19. Normalized S_{yz} shear stress contours at the interface of the center elastomeric layer and fiber reinforcement for isolators with interior modification diameter $d/2b =$ (a) 0, (b) 0.23, (c) 0.35 and (d) 0.58.
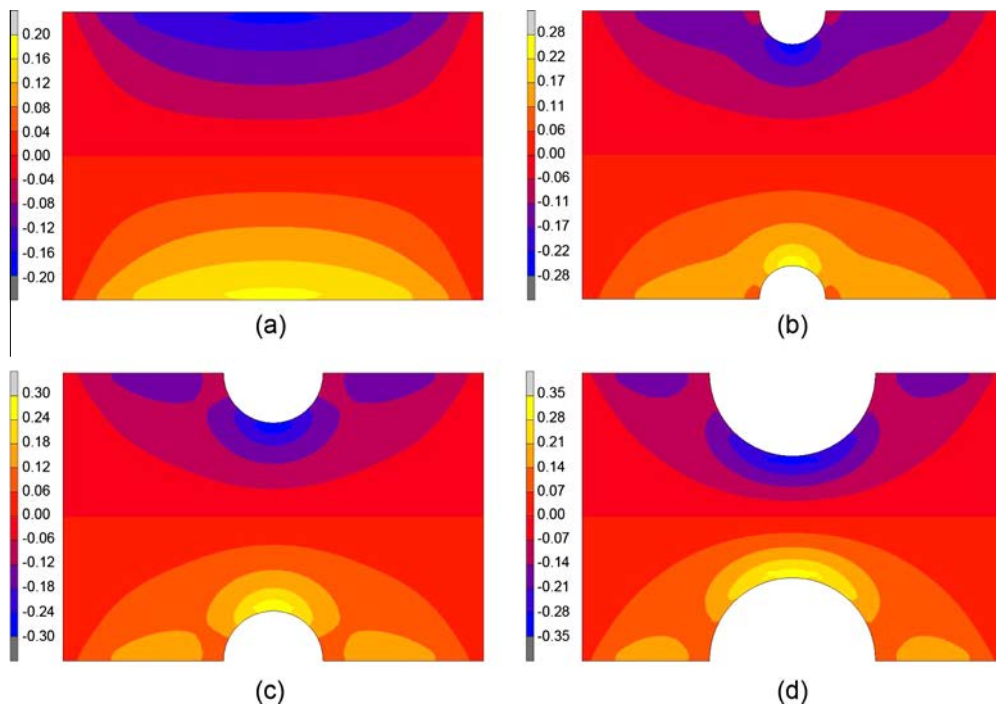

Fig. 20. Normalized S_{yz} shear stress contours at the interface of the center elastomeric layer and fiber reinforcement for isolators with exterior modification diameter $d/2b =$ (a) 0, (b) 0.23, (c) 0.35 and (d) 0.58.

5.6. Fiber reinforcement Von Mises stress

Figs. 21 and 22 show the Von Mises stress contours normalized by the average vertical pressure, $\sigma_v/\bar{p}$, in the center fiber reinforcement layers in the isolators with interior and exterior modifications, respectively. It can be seen that, similar to the observations made with the vertical stress distribution, introducing an interior modification causes a minor decrease in the peak value of $\sigma_v/\bar{p}$. As the diameter increases the peak value of $\sigma_v/\bar{p}$ also increases, exceeding the peak value of an unmodified isolator. For exterior modifications, a minor increase is immediately observed. This increase in $\sigma_v/\bar{p}$ continues until two peaks begin to form as seen with a diameter of $d/2b = 0.58$. The peak value of $\sigma_v/\bar{p}$ in the center fiber reinforcement layers is 10.5% and 11.1% greater than the
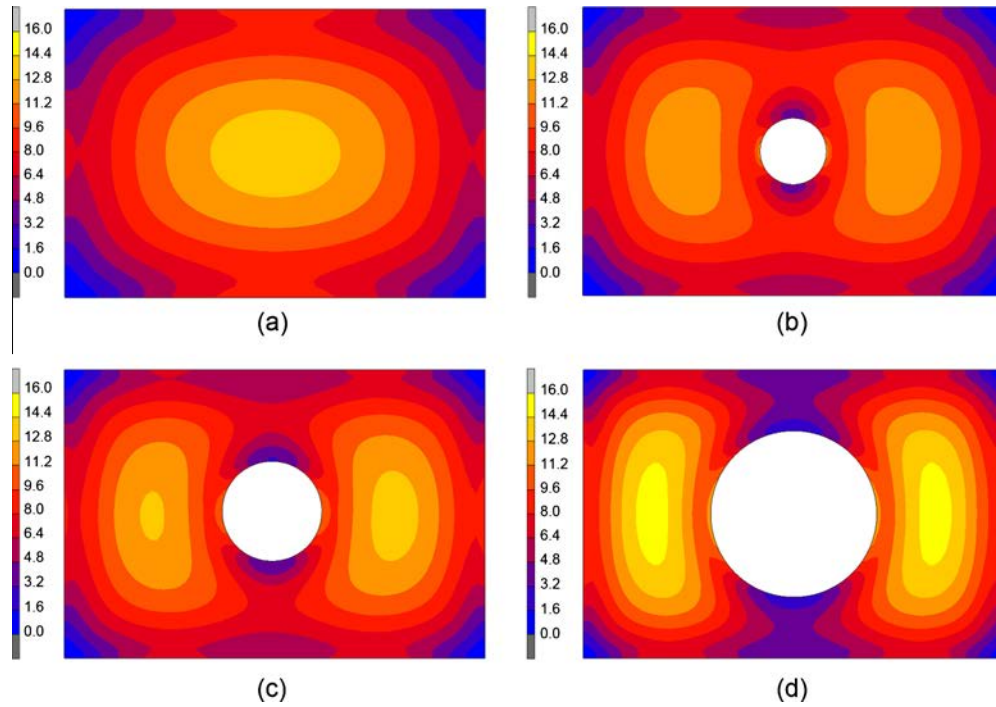

Fig. 21. Normalized Von Mises stress contours in center fiber reinforcement layers for isolators with interior modification diameter of $d/2b$ = (a) 0, (b) 0.23, (c) 0.35 and (d) 0.58.
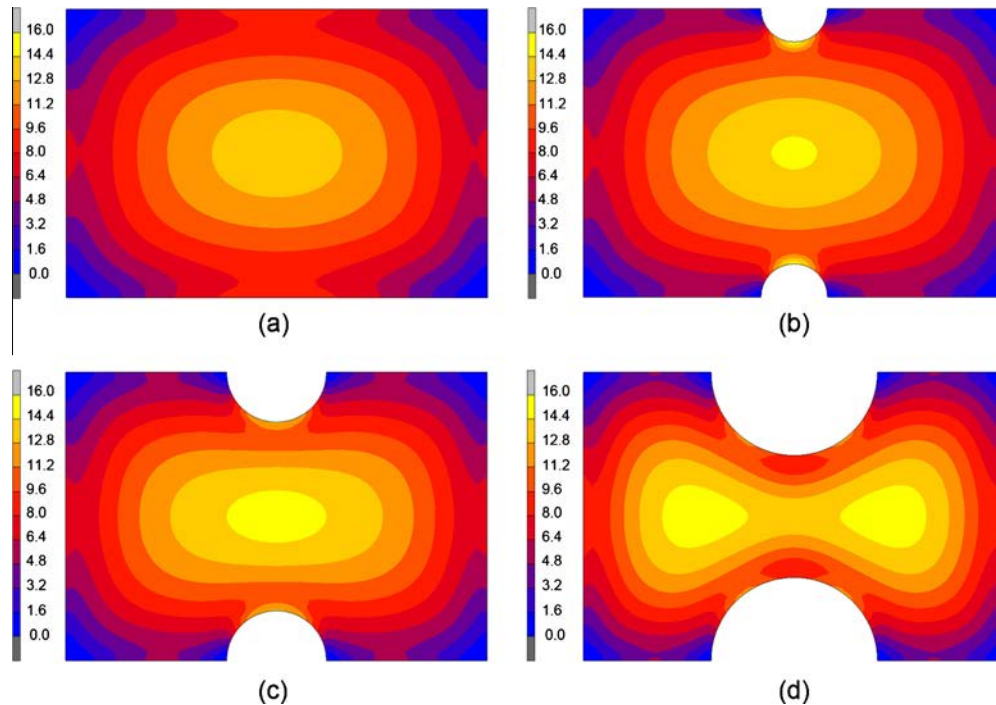

Fig. 22. Normalized Von Mises stress contours in center fiber reinforcement layers for isolators with exterior modification diameter of $d/2b$ = (a) 0, (b) 0.23, (c) 0.35 and (d) 0.58.

unmodified isolator at a diameter of $d/2b = 0.58$ for exterior and interior modifications, respectively.

6. Conclusions

This paper investigated the vertical behavior of unbonded Modified Rectangular Fiber-Reinforced Elastomeric Isolators (MR-FREIs). Experimental results were used to evaluate a three-dimensional finite element model. A parametric study was conducted on interior and exterior geometric modifications. It was found that both the vertical stiffness and compression modulus were highly sensitive to interior modifications and, to a lesser extent, exterior modifications. Similarly, the peak shear stress was also greater in isolators with interior modifications, and the peak shear stress usually occurred in the vicinity of the modification. The modifications generally increased the vertical stress and Von Mises stress distribution in the fiber reinforcement. As the diameter of the modification increased, the isolator began to behave as two individual isolators.

The primary purpose of MR-FREIs is to reduce the potentially high horizontal stiffness; consequently the horizontal behavior of MR-FREIs requires further investigation. An ongoing study by the authors indicates that the influence of modifications on the horizontal properties is displacement dependent, but a favorable decrease in horizontal stiffness and an increase in energy dissipation capability have been observed. Furthermore, the performance of a structure utilizing MR-FREIs, which has a direction-dependent horizontal stiffness, has yet to be investigated. It is expected that the modifications will provide designers with an additional parameter to optimize unbonded FREI design.

References

[1] Kelly JM, Konstantinidis D. Low-cost seismic isolators for housing in highly-seismic developing countries. In: ASSISi 10th World conference on seismic isolation, energy dissipation and active vibrations control of structures, Istanbul, Turkey; May 28–31; 2007.
[2] Kelly JM. Analysis of fiber-reinforced elastomeric isolators. J Seismol Earthq Eng 1999;2(1):19–34.
[3] Moon BY, Kang GJ, Kang BS, Kelly JM. Design and manufacturing of fiber reinforced elastomeric isolator for seismic isolation. J Mater Process Technol 2002;130–131:145–50.
[4] Moon BY, Kang GJ, Kang BS, Kim GS, Kelly JM. Mechanical properties of seismic isolation system with fiber-reinforced bearing of strip type. Int Appl Mech 2003;39(10):1231–9.
[5] Toopchi-Nezhad H, Tait MJ, Drysdale RG. Testing and modeling of square carbon fiber-reinforced elastomeric seismic isolators. Struct Control Health Monitor 2008;15:876–900.
[6] Toopchi-Nezhad H, Tait MJ, Drysdale RG. Lateral response evaluation of fiber-reinforced Neoprene seismic isolators utilized in an unbonded application. J Struct Eng ASCE 2008;134(10):1627–37.
[7] Toopchi-Nezhad H, Tait MJ, Drysdale RG. Bonded versus unbonded strip fiber reinforced elastomeric isolators: finite element analysis. Compos Struct 2011;93:850–9.
[8] de Raaf MGP, Tait MJ, Toopchi-Nezhad H. Stability of fiber-reinforced elastomeric bearings in an unbonded application. J Comp Mater 2011;45(18):1873–84.
[9] Van Engelen NC, Tait MJ, Konstantinidis D. Horizontal behaviour of stable unbonded fiber reinforced elastomeric isolators (SU-FREIs) with holes. In: Proceedings of the 15th world conference on earthquake engineering, Lisbon, Portugal; September 24–28; 2012.
[10] Kelly JM. Earthquake resistant design with rubber. 2nd ed. London: Springer; 1997.
[11] Constantinou MC, Kartoum A, Kelly JM. Analysis of compression of hollow circular elastomeric bearings. Eng Struct 1992;14(2):103–11.
[12] Kelly JM. Analysis of the run-in effect in fiber-reinforced isolators under vertical load. J Mech Mater Struct 2008;3(7):1383–401.
[13] Kelly JM, Konstantinidis D. Effect of friction on unbonded elastomeric bearings. J Eng Mech 2009;135(9):953–60.
[14] Kelly JM, Konstantinidis D. Mechanics of rubber bearings for seismic and vibration isolation. Chichester: John Wiley & Sons; 2011.
[15] Konstantinidis D, Kelly JM, Makris, N. Experimental investigation of the seismic response of bridge bearings. Report EERC-2008/02. Earthquake Engineering Research Center, University of California, Berkeley; 2008.
[16] Tsai HC, Kelly JM. Stiffness analysis of fiber-reinforced rectangular seismic isolators. J Eng Mech 2002;128(4):462–70.
[17] Pinarbasi S, Okay F. Compression of hollow-circular fiber-reinforced rubber bearings. Struct Eng Mech 2011;38(3):361–84.
[18] Pinarbasi S, Mengi Y. Elastic layers bonded to flexible reinforcements. Int J Solids Struct 2008;45:794–820.
[19] Tsai HC. Compression stiffness of infinite-strip bearings of laminated elastic material interleaving with flexible reinforcements. Int J Solids Struct 2004;41(24):6647–60.
[20] Tsai HC. Compression stiffness of circular bearings of laminated elastic material interleaving with flexible reinforcements. Int J Solids Struct 2006;43(11):3484–97.
[21] Tsai HC, Kelly JM. Buckling of short beams with warping effect included. Int J Solids Struct 2005;42:239–53.
[22] Tsai HC, Kelly JM. Buckling load of seismic isolators affected by flexibility of reinforcement. Int J Solids Struct 2005;42:255–69.
[23] Toopchi-Nezhad H, Tait MJ, Drysdale RG. Influence of thickness of individual elastomer layers (first shape factor) on the response of unbonded fiber-reinforced elastomeric bearings. J Comp Mater 2013;47(27):3433–50.
[24] Van Engelen NC, Tait MJ, Konstantinidis D. Vertical response behaviour of stable unbonded fiber reinforced elastomeric isolators (SU-FREIs) with holes in the loaded surface. In: Canadian society for civil engineering annual general conference. Edmonton, Canada; June 6–9; 2012.
[25] Dezfuli FH, Alam MS. Multi-criteria optimization and seismic performance assessment of carbon FRP-based elastomeric isolator. Eng Struct 2013;49:525–40.
[26] Foster BAD. Base isolation using stable unbonded fibre reinforced elastomeric isolators (SU-FREI): Master's thesis. Hamilton: McMaster University; 2011.
[27] Toopchi-Nezhad H, Tait MJ, Drysdale RG. Shake table study on an ordinary low-rise building seismically isolated with SU-FREIs (stable unbonded-fiber reinforced elastomeric isolators). Earthq Eng Struct Dyn 2009;38:1335–57.
[28] International Organization for Standardization. Elastomeric seismic-protection isolators, ISO 22762. Geneva: International Organization for Standardization; 2010.
[29] Warn GP, Whittaker AS, Constantinou MC. Vertical stiffness of elastomeric lead–rubber seismic isolation bearings. J Struct Eng 2007;133(9):1227–36.
[30] MSC Marc. Theory and user information, vol. A. Santa Ana: MSC Software Corporation; 2011.
[31] Osgooei PM, Tait MJ, Konstantinidis D. Three-dimensional finite element analysis of circular fiber-reinforced elastomeric bearings under compression. Comp Struct 2014;108:191–204.